



Contents lists available at ScienceDirect

International Journal of Applied Earth Observations and Geoinformation

journal homepage: www.elsevier.com/locate/jag

Multi-sensor remote sensing analysis of coal fire induced land subsidence in Jharia Coalfields, Jharkhand, India

Vamshi Karanam^{a,*}, Mahdi Motagh^{b,c}, Shagun Garg^b, Kamal Jain^a^a Department of Civil Engineering, Indian Institute of Technology Roorkee, 247667 Roorkee, Uttarakhand, India^b Remote Sensing and Geoinformatics, GFZ German Research Centre for Geosciences, 14473 Potsdam, Germany^c Institute for Photogrammetry and Geo-Information, Leibniz University Hannover, 30167 Hannover, Germany

ARTICLE INFO

Keywords:

Coal mining
Coal fires
Land subsidence
Land surface temperature
Temperature anomaly
Persistent scatterer interferometry

ABSTRACT

The subsidence in coal mines induced by surface and subsurface fires leading to roof collapse, infrastructure loss, and loss of lives is a prominent concern. In the study, satellite imagery from thermal and microwave remote sensing data is used to deduce the effect of coal fires on subsidence in the Jharia Coalfields, India. The Thermal Infrared data acquired from the Landsat-8 (band 10) is used to derive the temperature anomaly maps. Persistent Scatterer Interferometry analysis was performed on sixty Sentinel-1, C-band images, the results are corrected for atmospheric error using Generic Atmospheric Correction Online Service for InSAR (GACOS) atmospheric modelling data and decomposed into vertical displacement values to quantify subsidence. A zone-wise analysis of the hazard patterns in the coalfields was carried out. Coal fire maps, subsidence velocity maps, and land cover maps were integrated to investigate the impact of the hazards on the mines and their surroundings. Maximum subsidence of approximately 20 cm/yr. and temperature anomaly of up to 25 °C has been observed. The findings exhibit a strong positive correlation between the subsidence velocity and temperature anomaly in the study area. Kusunda, Keshalpur, and Bararee collieries are identified as the most critically affected zones. The subsidence phenomenon in some collieries is extending towards the settlements and transportation networks and needs urgent intervention.

1. Introduction

The efficiency of a country's industries and production largely depends on the natural sources of energy. Coal mines are the lifeline for electricity generation, accounting for 38.4% of the world's total electricity production (Bódis et al., 2019; World Energy Outlook, 2018). However, contamination of air, water, and soil due to the coal mines result in severe health problems for the surrounding neighbourhoods. With improper planning and inefficient executions, the issues also multiply to include coal fires, land subsidence, and roof collapse, which unfortunately has become a frequent scenario.

Coal fires, ignited by forest fires, lightning strikes, or human actions, are significant causes of subsidence in coal mines (Chatterjee et al., 2007). Coal fires burn the underground coal and create voids leading to land subsidence, which in turn aggravates the coal fires by creating cracks and fissures at the surface that serve as inlets for oxygen. Also, gases formed due to subsurface coal fires create pressure resulting in cracks and surface uplift (Rosema and van Genderen, 1995). Mine

subsidence shows a localized pattern as the mining generally does not cover a large area. The order of subsidence varies with the method of surface or underground mining employed. Sometimes multiple factors such as illegal and undocumented mining, coal fires, illegal settlements, type of soils, etc., come together to accelerate the subsidence phenomenon. When continued for long intervals, this subsidence may lead to roof failure and eventually collapse. Coal fires directly impact the environment, coal reserves, and coal mine workers and indirectly affect the economy of the country and the safety and well-being of society. Inundation is also a significant hazard in coal fields, filling the hollow undergrounds with water due to the sudden rush of surface water into the mines, especially during monsoon season (Bringemeier, 2012). The risk due to mine inundation is a threat to mine workers as the sudden inrush of water prevents their escape from underground mines and traps them. Deng et al., 2017 has identified 105 coal mine risks, out of which coal fires and roof collapse are identified as the most severe risks, and controlling them could help decrease 26% and 33% of the total risk factor, respectively. During 1947–2010, nearly 60% of the disasters in

* Corresponding author at: Department of Civil Engineering, Indian Institute of Technology Roorkee, 247667 Roorkee, Uttarakhand, India.

E-mail addresses: vk@ce.iitr.ac.in (V. Karanam), motagh@gfz-potsdam.de (M. Motagh), shagun@gfz-potsdam.de (S. Garg), kamal.jain@ce.iitr.ac.in (K. Jain).

<https://doi.org/10.1016/j.jag.2021.102439>

Received 12 February 2021; Received in revised form 1 July 2021; Accepted 4 July 2021

Available online 17 July 2021

1569-8432/© 2021 The Authors. Published by Elsevier B.V. This is an open access article under the CC BY license (<http://creativecommons.org/licenses/by/4.0/>).

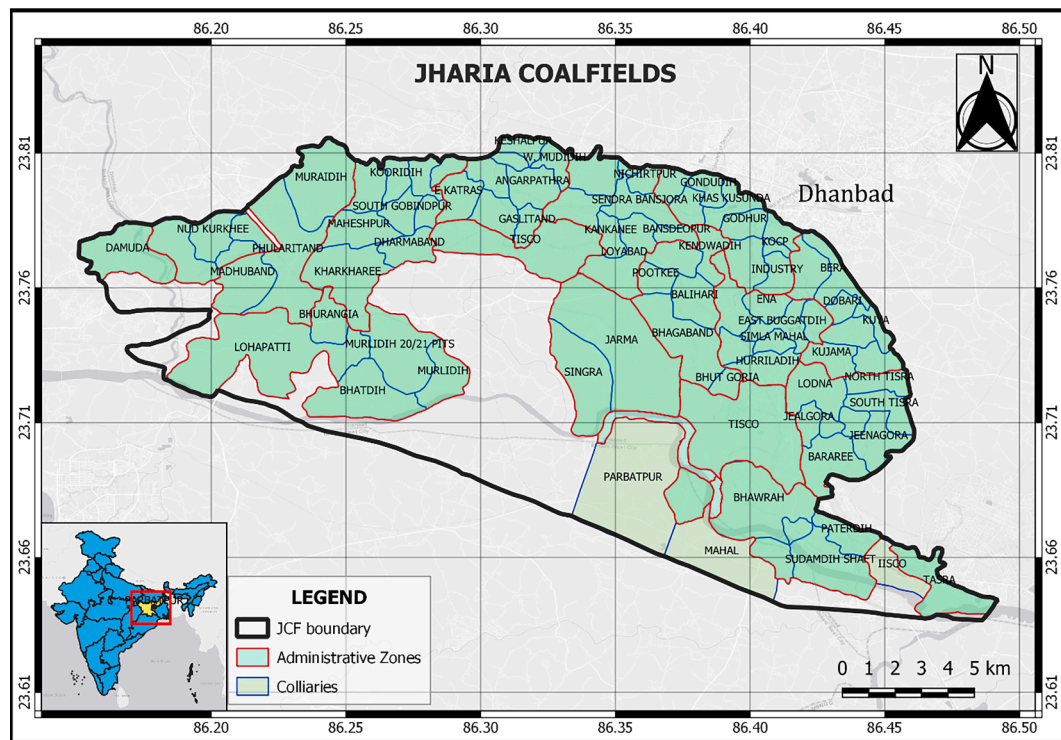


Fig. 1. Jharia Coalfields.

the coal mines in India are due to coal mine fire, explosion, subsidence and roof collapse. Roof falls account for more than a quarter of deaths in coal mines (Kumar and Pathak, 2001).

With the increase in demand for coal due to the industrial revolution, illegal and unplanned mining also increased in India. Sometimes the old and abandoned mines go untraced due to the unavailability of the mines' records (Chatterjee et al., 2016; Singh and Dhar, 1997). This has led to several disasters in the mining areas and substantially damaged the infrastructure, coal resources, and lives (Gupta et al., 2013; Prakash et al., 2010). Jharia Coalfields, the largest and one of India's oldest coalfields, is home to precious prime coking coal in the country. They are critically affected by coal fires leading to subsidence due to their poor management in the past. In JCF, the first coal fire was reported more than a century ago, in 1916 (Pandey et al., 2016). Coal fires are so frequent that they consumed more than 2 million tonnes of coal between 2018 and 2020 (Limited, 2020). Currently, about 70 fires are burning in the Jharia coalfield, which is the highest among all coalfields in India (Chatterjee et al., 2015; Stracher and Taylor, 2004). There have been several incidences of damages due to the coal fires and subsidence. Transportation lines are abandoned, houses are affected, and thousands of people are displaced. Most recently, in Dec 2020, a woman was burnt alive after being sucked into a hole created due to a sudden roof collapse caused by fires underneath. Due to the severity of the coal fires and the subsidence induced by them, a detailed analysis of these hazards is necessary.

Traditional coal fire detection methods using handheld radiometers, thermocouples, Boreholes, temperature loggers, and other geophysical methods are time-consuming and require human presence near the burning fires and unreachable areas (Gangopadhyay et al., 2012; Kuenzer et al., 2008). Alternatively, satellite thermal imagery had become a vital tool to identify the fires and temperature changes over a large area from a relatively safer distance by exploiting the relation between the emissivity and radiant temperature. Using this technique, several researchers have identified and quantified the surface and sub-surface coal fires in the mines (Chatterjee, 2006; Saraf et al., 1995; Singh et al., 2017; Zhang et al., 2004).

Simultaneously, DInSAR (Differential Interferometric Synthetic Aperture Radar) has become a powerful tool to calculate and monitor land deformations caused by various natural and human-made activities (Haghighi and Motagh, 2017; Massonnet and Feigl, 1998; Motagh et al., 2007, 2008, 2017; Rosen et al., 2000). It uses the phase components of two or more Synthetic Aperture Radar (SAR) images to generate the interferogram and extract the deformation volume and intensity (Crosetto et al., 2016). SAR technology has taken a new turn with the Sentinel 1A and 1B constellation on-board since the data provided is open source and covers almost the entire world. However, DInSAR is prone to errors due to atmospheric interactions and noise. This can be minimized by combining several interferograms and generating time-series information. Advanced InSAR time-series techniques such as Persistent Scatterer Interferometry (PSI) and Small Baseline Subset (SBAS) can measure continuous deformations up to millimetre level (Agarwal et al., 2020; Awasthi et al., 2020; Bernardino et al., 2002; Crosetto et al., 2016; Haghshenas Haghighi and Motagh, 2019).

Various studies have used advanced DInSAR techniques to estimate the coal-fire induced subsidence. For example, Jiang et al., 2011 used PSI, stacking and 2-Pass DInSAR techniques to measure the subsidence in Wuda coalfield, Northern China using ENVISAT ASAR images. The results are compared to the coal fire data obtained from field surveys, and the effect of subsidence on coal fire zones is estimated. The results also highlight the development of new coal fire areas leading to new subsidence zones. Zhou et al., 2013 used ALOS-PALSAR data to calculate the deformation in the Wuda coalfields by stacking method and compared it with the coal fire maps obtained from fieldwork and found several locations affected by both hazards. Liu et al., 2019 has combined the Persistent Scatterers (PS) and Distributed Scatterers (DS) to estimate the subsidence in Miqian Coal Fire Zone in Xinjiang, China. The subsidence results accurately match the coal fire point information obtained from drilling technology. Pinto et al., 2014 used a stack of 19 TSX Stripmap images for the PS analysis covering the dry season in the Azul open pit manganese mine located in Carajás Province, Amazon region and detected significant land subsidence over the north waste pile region.

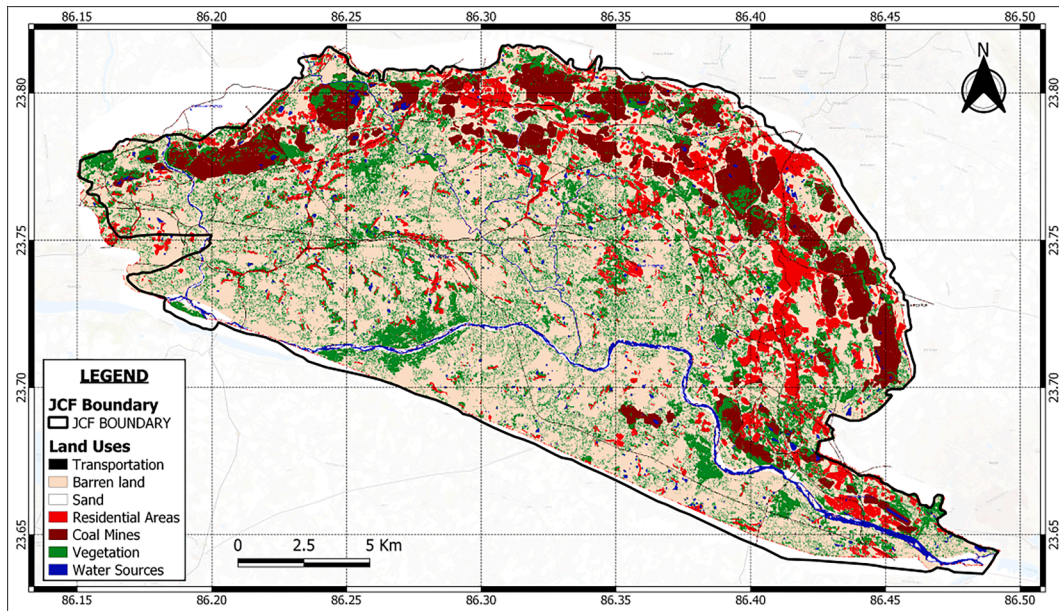


Fig. 2. Land Cover map of Jharia Coalfields.

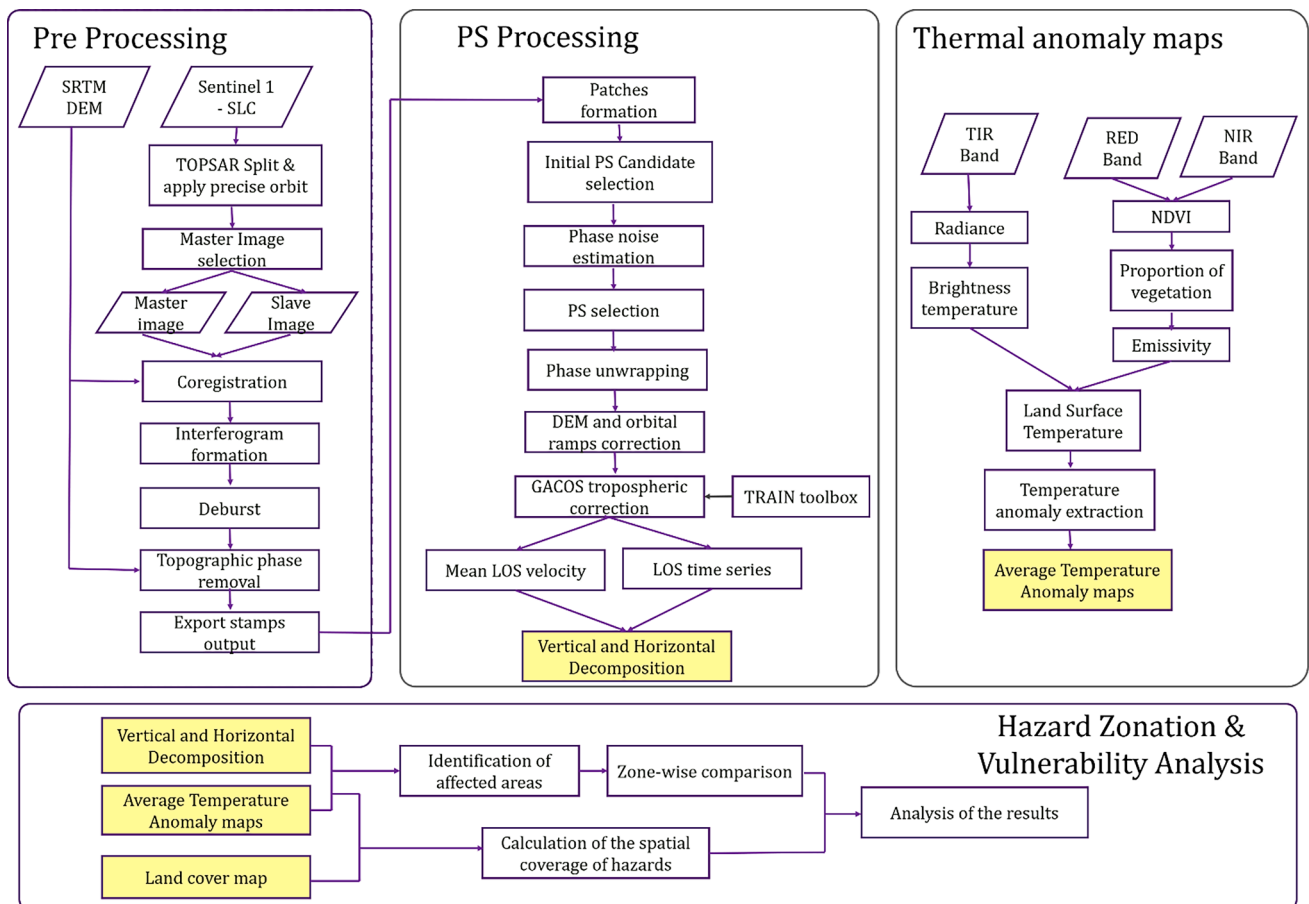


Fig. 3. Methodology chart.

Since the 1990s, several studies on coal fires and land subsidence in Jharia have been conducted using thermal and radar remote sensing. Chatterjee et al., 2010 used InSAR coherence and phase information to delineate the un-reclaimed, abandoned or closed opencast mines from active opencast mines with spectral signature analysis of optical

imagery. Chatterjee et al., 2015 has compared the efficiency of ALOS-PALSAR (L band), ENVISAT (C band) imagery, GPS, and Precision levelling for monitoring the fast-moving and slow-moving subsidence regions in the Jharia Coalfield. Mishra et al., 2020 delineated coal fires at JCF using iterative techniques with the help of Landsat imagery

captured between 2001 and 2016. They observed that even though the coal-fire affected area remained the same, only 12% of the coal fires in 2001 continued burning, meaning that the fires spread to new places. Roy et al., 2015 identified that the wintertime Landsat-8 imagery could detect the coal fires in JCF effectively.

In this research, coal fires and subsidence in the Jharia Coalfields are investigated using thermal imagery and SAR imagery. For the first time, we have estimated the intensity, spatial coverage and temporal evolution of the coal fires and land subsidence in Jharia Coalfields and evaluated the correlation between the two hazards. We have used the latest satellite remote sensing observations from Sentinel-1 and Landsat-8 to overcome the limitations in the datasets used by previous studies, such as large temporal baseline and limited acquisitions. The subsidence and coal fire phenomenon in the JCF is limited to few locations. Thus, we identified the individual collieries based on the hazard patterns to highlight the hazard scenario in each zone. Further, we performed a deeper analysis of each hazard zones. Our study can form a basis to focus on the critical collieries for further studies and in implementing disaster management measures.

2. Study area

Jharia coalfields (JCF), named after the significant coal-bearing town, Jharia, in Dhanbad district of Jharkhand state, India, covers about 400 sq. km between 86°05' – 86°30' East and 23°35' – 23°55' North (see Fig. 1). Nearly half a million people reside in the 58 villages inside the coalfield region. The Jharia coalfields are divided into 18 administrative zones and 89 collieries. They are home to 9 opencast mines and 31 underground mines. The mining techniques used here are the board and pillar technique and longwall mining. 80–100 million tonnes of coal is produced every year with the help of nearly 50,000 workforces (Limited, 2020).

A land cover map of the study area is shown in Fig. 2. Damodar river passes through the southern end of the coalfields. Transportation, including roads and railways, is predominantly in the northern part of the study area. Most of the study area is occupied by barren lands, while coal mines lie in the North and East parts. Residential areas are near to the mines since most people are employed in the coalfields. Vegetation includes farmlands, parks, forests, and reclamation sites that are converted into gardens. The topography of Jharia is nearly flat, and hence the effect of differential solar heating can be neglected.

The lower part of JCF consists of exposed Gondwana rocks. The crystalline gneiss surrounds Gondwana strata. The strata consist of rocks belonging to Talchir and Damuda series. Damuda series include Raniganj series, barren measures and Barakar series. In the western part, Dolerite dykes, and in the barakar formation, mica-peridotite dykes and sills are present (Verma et al., 1979). Barakar series in the North and Eastern part of the coalfields are actively being mined and are prominent for coal fires. Raniganj series in the south-western part of the coalfields have suffered much subsidence, and the mining in this area is now highly tricky. The general dip angle of the formation is 10 with up to 70 at certain places near the southern boundary fault (Borah et al., 2017). The strike of the formation is West-Southwest to East-Northeast in general (Cell, 2017). The thickness of the coal seams is up to 4.8 m in one lift and goes up to 12 m for multi lift and multi-section mining. The average depth of the underground workings is 250 m (Saxena, 1991).

3. Methodology

For the study, satellite imagery from thermal and microwave regions of the electromagnetic spectrum is used. The study is divided into two phases to monitor the change in the coal fire and subsidence phenomenon. Phase-I includes November 2017- April 2018, and phase-II is from November 2018 to April 2019. Data from the winter season is used to minimize the errors due to differential solar heating and atmospheric interactions. A flowchart for the methodology is presented in Fig. 3.

3.1. Thermal remote sensing

The thermal Infrared data acquired from the Landsat-8 thermal band (band 10) is used to derive the temperature anomaly maps of the study area (Table A1). The spatial resolution of the Thermal Infrared Imaging Spectrometer (TIRS) is 100 m.

Upon touching the surface of a body, some part of the incident radiation gets absorbed and later emitted from the body depending upon the object's emissivity to maintain temperature equilibrium. Thermal remote sensors such as TIRS capture and store the top of the atmosphere electromagnetic radiation, which lies between 8 and 14 μm and 3–5 μm wavelength region, emitted by the target. The relationships between the electromagnetic radiation and the kinetic temperature of the body can be exploited to compute the Land Surface Temperature (LST) using the emissivity information obtained with the help of Planck's constant, Boltzmann's constant, and NDVI values of the target area.

The temperature data from TIRS images, stored as digital numbers, are converted to atmospheric radiance values using the emission resistance factor. The Satellite Brightness Temperature is calculated from the top of the atmosphere radiance values in the next step. Using the NDVI image from Red and NIR bands, land surface emissivity is calculated. And then, emissivity is calculated from the land surface emissivity values. Finally, LST is computed using at-satellite brightness temperature (BT), operating wavelength of the sensor, and emissivity (e) as given in equation (1).

$$LST = \left(\frac{BT}{1 + \lambda \left(\frac{BT}{1.4388} \right)} \right) * \ln(e) \quad (1)$$

3.2. InSAR analysis

Sixty (60) Sentinel-1 images (Tables A2 and A3) captured in ascending and descending directions are obtained for the PSI analysis using the Stanford Method for Persistent Scatterers (StaMPS) method (Hooper et al., 2012). The PSI method implemented in StaMPS exploits a PS selection algorithm using phase characteristics to identify PS in natural terrains. Moreover, it does not require a priori deformation model (Hooper et al., 2010).

Several steps are involved in the pre-processing of SAR data. Initially, precise orbit files are applied to the Sentinel images. Appropriate bursts covering the study area are selected, and TOPSAR Split is carried out. Later, the best master image is chosen considering the temporal baseline, perpendicular baseline, and least atmospheric interaction and co-registered with all the slave images of the particular phase. This co-registered stack is used to generate interferograms by cross-multiplication of the master image with the slave images. Further, the DInSAR images are created by subtracting the topographic component from the interferograms using three arcsec resolution (90 m) Shuttle Radar Topography Mission (SRTM) DEM. SNAP (SentiNel Application Platform) was used for the pre-processing (Blasco et al., 2019).

Pre-processing is followed by Persistent Scatterer Analysis as implemented in the StaMPS method (Hooper et al., 2012). Initially, an amplitude dispersion index of 0.4 is chosen for identifying the permanent scatterers. For every interferogram, the phase noise value is estimated using the Combined Low-pass Adaptive Phase (CLAP) filter for the given filter grid. This is an iterative process. After that, based on the noise characteristics estimated in the previous step, the PS points are filtered. Some pixels whose amplitude is due to the contribution from the neighbouring ground resolution elements are weeded out to reduce the noise. Spatially uncorrelated look angle (SULA) is corrected in the wrapped phase information of PS points. Phase unwrapping of the PS points is done at a grid size of 50 m \times 50 m using the 3D unwrapping method. Further, spatially correlated DEM error due to the inaccurate DEM or imprecise mapping of DEM to the Radar coordinates is estimated

Table 1
Classification of the subsidence and coal fire hazards.

Land subsidence (in cm/yr.)	Temperature anomaly (in °C)	Classification
> -10	>10	Very High
-10 to -5	5 to 10	High
-5 to -1 & > +1	1 to 5	Medium
-1 to +1	<1	Low

and removed. The atmosphere component and orbital component in the master image are also calculated in this step. Finally, the atmospheric filtering of the unwrapped interferograms is performed. The results from the analysis include wrapped and unwrapped interferograms, estimations for atmospheric, orbital, DEM errors, velocity maps, and time series maps.

The interferograms are corrected using GACOS atmospheric modelling data to minimize the errors due to atmospheric interactions in the PSI results. Generic Atmospheric Correction Online Service for InSAR (GACOS) by New Castle University provides high spatial resolution zenith tropospheric delay maps for the InSAR tropospheric corrections (Yu et al., 2018). Atmospheric sounding data provided by the University of Wyoming consists of the details of the atmosphere’s physical properties, such as temperature, pressure, wind speed, wind direction, etc., twice a day, every day, for selected locations. For the study, sounding data of the nearest station, Ranchi, and the GACOS atmospheric modelling data covering the study area are collected. Toolbox for Reducing Atmospheric InSAR Noise (TRAIN) package is employed to perform atmospheric noise removal using GACOS atmospheric modelling data (Bekaert et al., 2015). Initially, Refractivity, the mean LOS delay, and the displacement are computed based on the given processing parameters such as the wavelength of the SAR data, look angle and sounding data, etc... For each GACOS image, a zenith tropospheric dry and wet delay is computed. Interferometric phase delays are calculated and subtracted from the interferogram stack using the look angle and wavelength.

The subsidence information obtained from the ascending and descending datasets after all the corrections is the line-of-sight deformation, meaning that the deformation is either towards or away from the side looking satellite. Hence, the information should be decomposed into vertical and horizontal deformation values for quantitative analysis. Initially, the ascending (d_{asc}) and descending (d_{dsc}) datasets are cross

multiplied using the header angle (α) of the satellite and incidence angle (Θ) of the pixel to generate vertical (d_{ver}) and horizontal (d_{hor}) deformation maps using Eq. (2). The generated vertical subsidence map represents the deformation along the nadir line, while the horizontal deformation map represents the deformation along the Earth’s horizontal surface.

$$\begin{pmatrix} d_{asc} \\ d_{dsc} \end{pmatrix} = \begin{pmatrix} \cos\Theta_{asc} & -\cos\Theta_{asc}\sin\Theta_{asc} \\ \cos\Theta_{dsc} & -\cos\Theta_{dsc}\sin\Theta_{dsc} \end{pmatrix} \begin{pmatrix} d_{ver} \\ d_{hor} \end{pmatrix} \quad (2)$$

3.3. Hazard zonation and vulnerability analysis

In JCF, each colliery or group of collieries have their mining plan and execution methods. Thus, the subsidence phenomenon in each region is independent and have no connection with the others. So, to study each hazard area more effectively, it is divided into zones. The zones are divided based on the results obtained from remote sensing observations. Each zone comprises one or more collieries affected by the hazards. The subsidence area and velocity are calculated for each phase and compared between each other. The effect of these hazards on the neighbouring population and infrastructure is discussed.

The area under the influence of coal fire and land subsidence hazards is extracted, and the spatial coverage of both hazards is calculated by integrating the land subsidence map and coal fire map. The hazards are classified into four: low, medium and high and very high, to provide a comprehensible visual interpretation of their distribution. Subsidence velocities less than 1 cm/yr are identified as background noise by visual inspection. The impact of subsidence beyond 10 cm/yr is dangerous even in locations with minimal human presence. The areas with high-temperature anomaly are either surface fires or high intense sub-surface fires. Information on the classification of hazard levels is provided in Table 1.

Later, this hazard map is overlaid on the land cover map to identify the vulnerable areas. A land cover map (Fig. 2) is prepared using Indian Remote Sensing satellite imagery, and a ground survey is regenerated using unsupervised classification methods and GIS techniques (Cell, 2017). The different land cover areas over the different hazard levels are calculated to help understand the extent of potential damage. It communicates the information on vulnerable areas prone to concerning hazards.

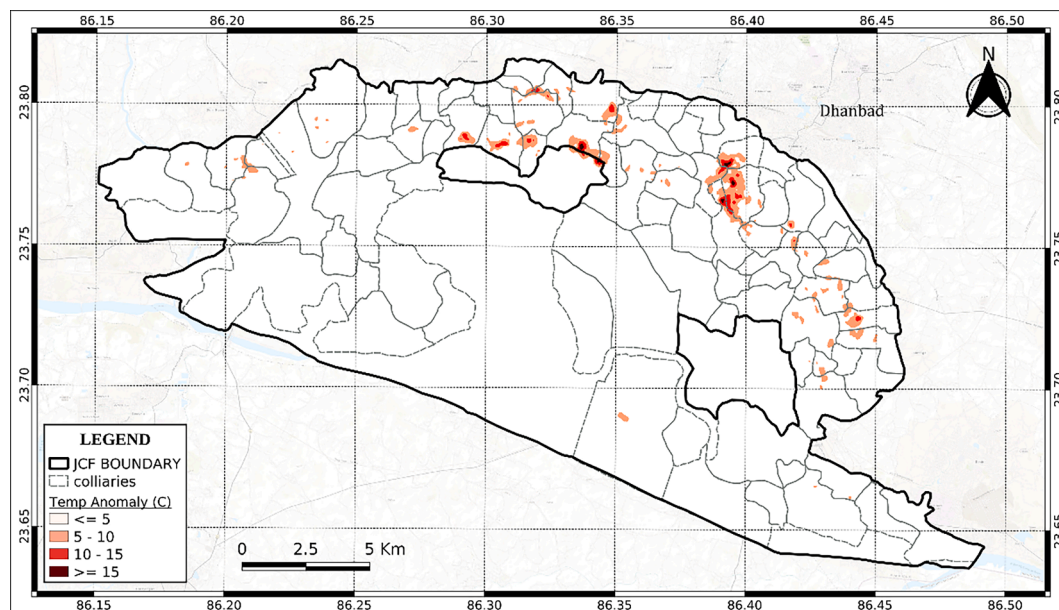


Fig. 4. Average temperature anomaly map of the study area for phase-I.

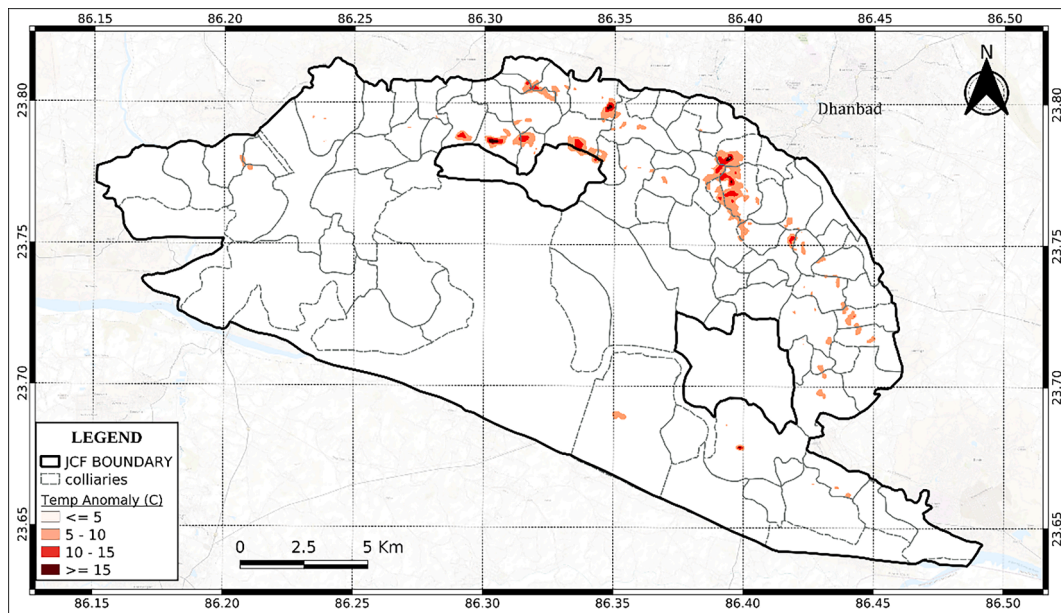


Fig. 5. Average temperature anomaly map of the study area for phase-II.

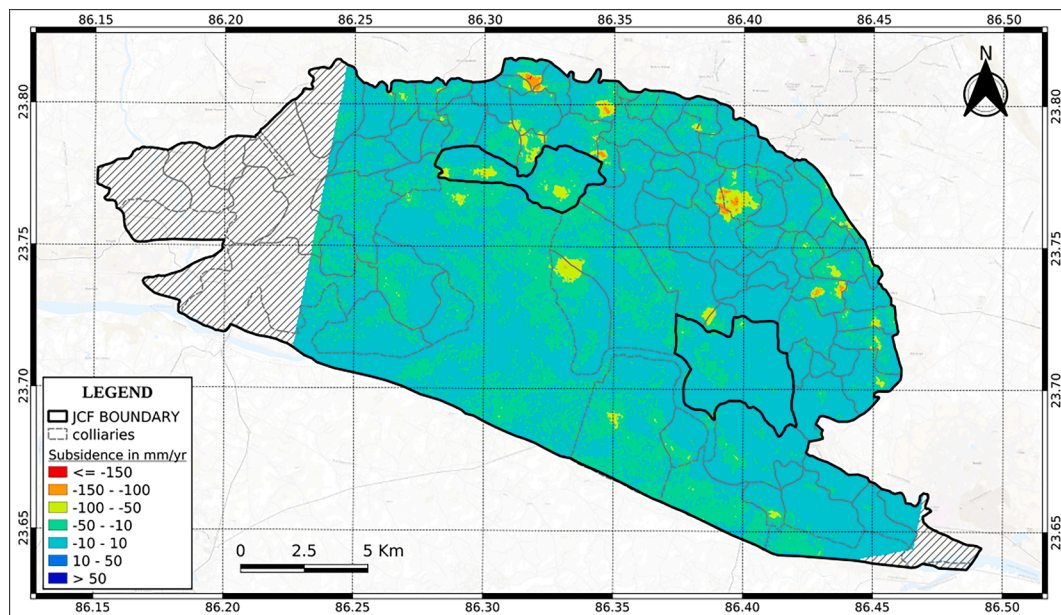


Fig. 6. Vertical subsidence for Phase-I in Jharia Coalfields.

4. Results and discussion

4.1. Coal fire maps

The generated LST map represents the temperature of the study area at the Earth’s surface. Several such maps for the study period are calculated. The difference between the pixel values of LST maps for no-fire regions in the winters and the no fire regions in the summers is significant due to the difference in Sun’s radiation. For example, in the phase-I data from Table A1, the maximum temperature for the study area in Dec 2017 imagery was 40 °C, while the same in the April 2018 imagery was 55.6 °C. To normalize this, the temperature values in each image are subtracted from a reference area with no active fires and constant emissivity values to determine the temperature anomaly in the study area. Due to the high density of stable features such as buildings

and infrastructure, the emissivity value of objects in the chosen reference area, Dhanbad city, remains constant throughout. Several such temperature anomaly maps are averaged together to generate an average temperature anomaly map.

The results presented in Figs. 4 and 5 show the presence of most coal fires in the northern and north-eastern side of the study area where the mining is actively taking place. The temperature anomaly range varies between −10 °C and +25 °C. The negative values belong to the Damodar river area, while the coal mines show maximum temperature anomaly. The areas with a significant temperature anomaly of more than 10 °C are considered to be affected by coal fires. Small regions inside these coal fire-affected areas portray the zones with the highest temperature anomaly of up to 20 °C, explaining the intense coal fire phenomenon. Due to the large pixel size of TIRS data, each pixel receives information from both fire regions and non-fire regions, which explains the lower

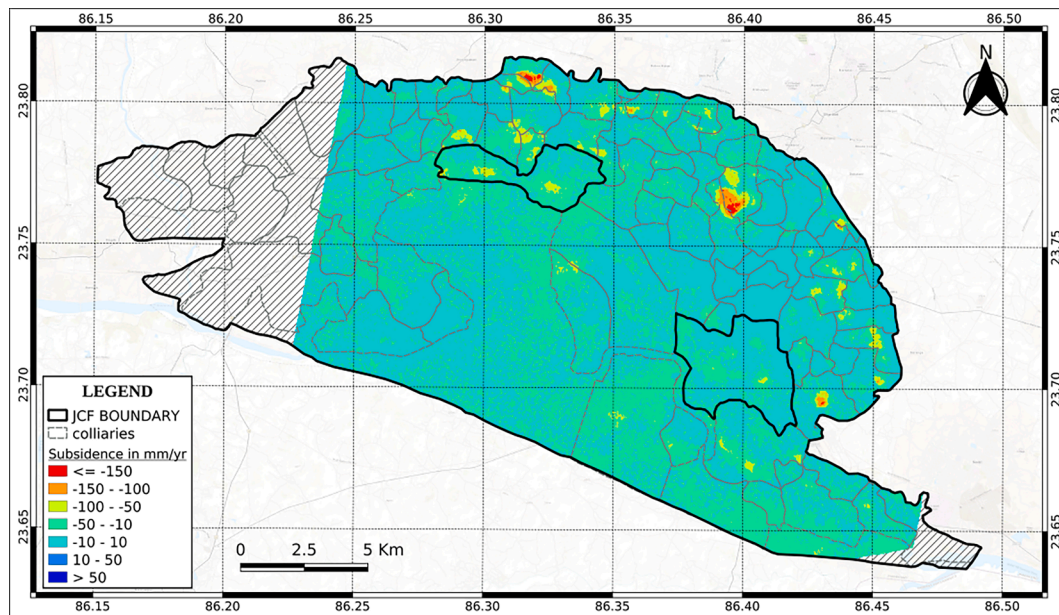


Fig. 7. Vertical subsidence for Phase-II in Jharia Coalfields.

Table 2

Division of collieries according to subsidence zones.

COLLIERY	ZONE
Keshalpur, Ram Kanali, W. Mudidih	Zone-I
Katras Choitudih, Gaslitand, Angarapatra	Zone-II
Kusunda, Kustore	Zone-III
East Katras	Zone-A
Bararee	Zone-B

temperature anomaly values. Areas with the highest coal fires lie in the Kusunda, Keshalpur, Mudidih, Katras Choitudih, and Tetulmari collieries. The spread of coal fires remained almost the same for the two years except for keshalpur and Bararee collieries, where new fire zones have emerged. Some collieries like Katras Choitudih, Tetulmari, and Gaslitand have seen an increase in the intensity of coal fires between the two phases.

4.2. Subsidence maps

PSI analysis was carried out on the single-master interferogram stack. In phase I, 1,310,826 PS points are identified for the ascending dataset, while 764,230 PS points are identified for the descending dataset. Similarly, 1,408,333 PS points and 899,497 PS points were identified in Phase-II's ascending and descending dataset. Unwrapping of the interferograms and subsequent analysis was executed on these PS points. After the images are unwrapped, interferograms severely affected by the atmosphere errors were removed using GACOS imagery, and line of sight (LOS) velocity maps were computed. A similar analysis was carried out for the remaining dataset. These results were decomposed to generate vertical subsidence maps. The standard deviation of the results outside the main deformation zone is computed to check for the reliability of the data. We observed a standard deviation of 1.3 cm/yr, which is nearly 20 times less than the deformation range observed in the study. We have also analyzed the scatterplots to determine the correlation between the ascending and descending results (Supplementary Figure 1). The results show a strong positive correlation.

Figs. 6 and 7 are the vertical subsidence maps for the two phases of the study period. Several localized patterns of subsidence are recorded in the coalfields. The significant subsidence phenomenon is taking place in the northern and eastern parts of the coalfields. Jharia Coalfields is

subsiding at an average rate of 10 cm/yr to 20 cm/yr. Major subsidence points belong to Kusunda, Keshalpur, Tetulmari, Gaslitand, and Bararee collieries, where mining is actively taking place. In the southern and central part of the coalfields, where the rocky surface is prevalent, and the scope of mining is limited, the least amount of subsidence is reported. However, the emergence of a new subsidence zone in Bararee implies that the subsidence is extending towards the southern parts of the coalfield.

4.3. Zone-wise analysis of coal fires and subsidence

There are several subsidence zones in different parts of the coalfield. Zooming into each zone and analyzing them individually can offer detailed information on their subsidence and coal fire phenomenon. So, the subsidence maps and coal fire maps are divided into five different zones, as shown in Table 2. Each zone comprises one or more collieries affected by subsidence. In Phase-I of the study period, three major subsidence zones were identified over the Keshalpur, Gaslitand and Kusunda mines. All of the zones are in the northern and eastern parts of the study area. In Phase-II, two new subsidence zones belonging to East Katras colliery of the central region, Bararee colliery in the southeastern region, were identified. A different naming convention is given for the hazard zones identified in Phase-I (Zones I, II & III) and the hazard zones identified in Phase-II (Zones A & B). Vertical subsidence maps and coal fire maps of both the phases for each zone are compared to derive the relation between them. Time-series graphs for significant points over each subsidence zone are prepared for visualizing the intensity of subsidence in both phases.

4.3.1. Zone-I (Ramkanali, Keshalpur, and West Mudidih)

Zone-I comprises Ramkanali, Keshalpur, and West Mudidih collieries (Fig. 8). There is a minimal presence of settlements in the region, and the subsidence is limited to coal mines. Some reclamation sites inside the coal mine region are also affected. The major part of the subsidence is noticeable in the Keshalpur colliery with a velocity of up to 15 cm/yr. The subsiding area is spread over 0.8 sq. km, while the coal fires are also prominent in the colliery. Though the subsidence zone occupies a broader area, it coincides with the coal fire region with a temperature anomaly up to 15 °C. Between the two phases, the northward movement of the subsidence phenomenon with an increased velocity of up to 20 cm/yr is observed. The coal fire maps show the increase in the extent of

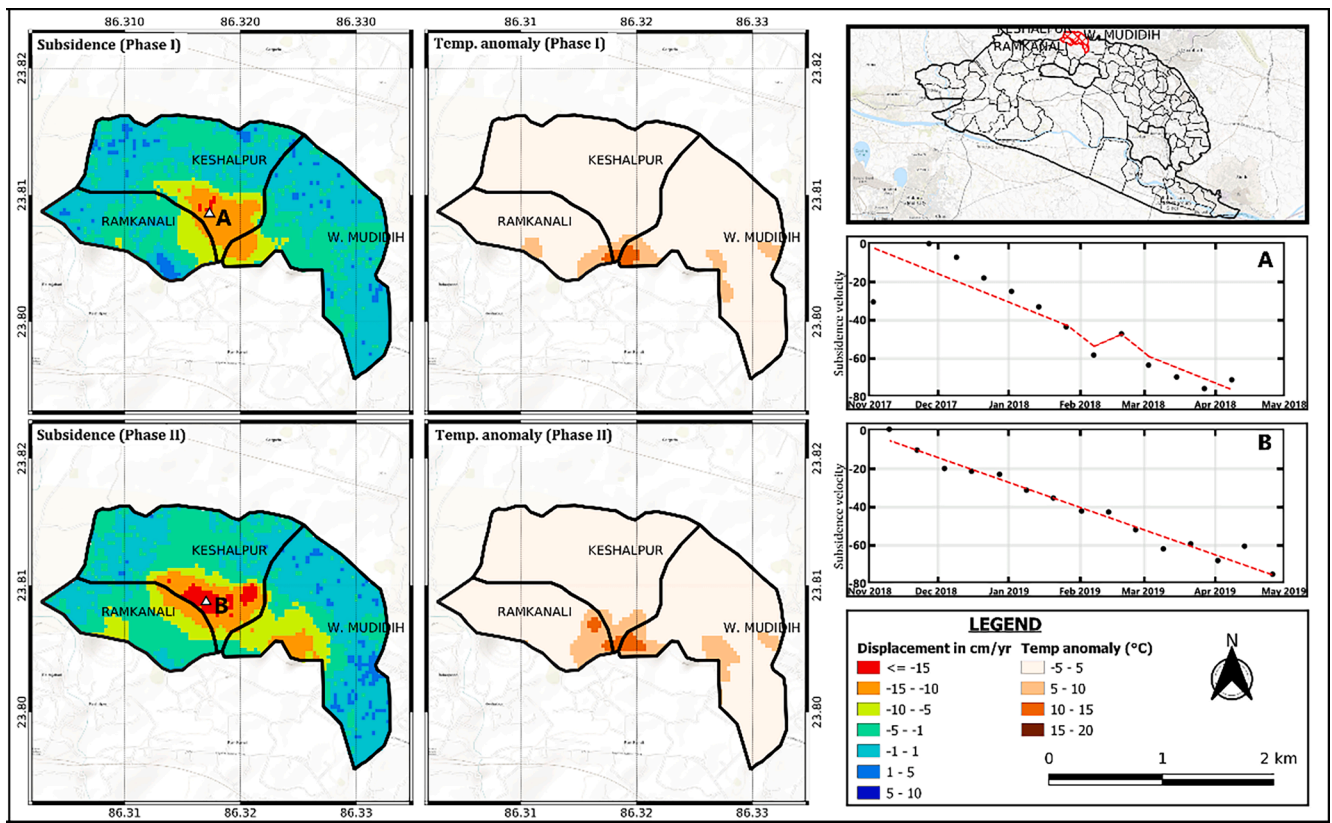


Fig. 8. Spread of coal fire and subsidence hazards in Keshalpur, Ramkanali and West Mudidihi collieries.

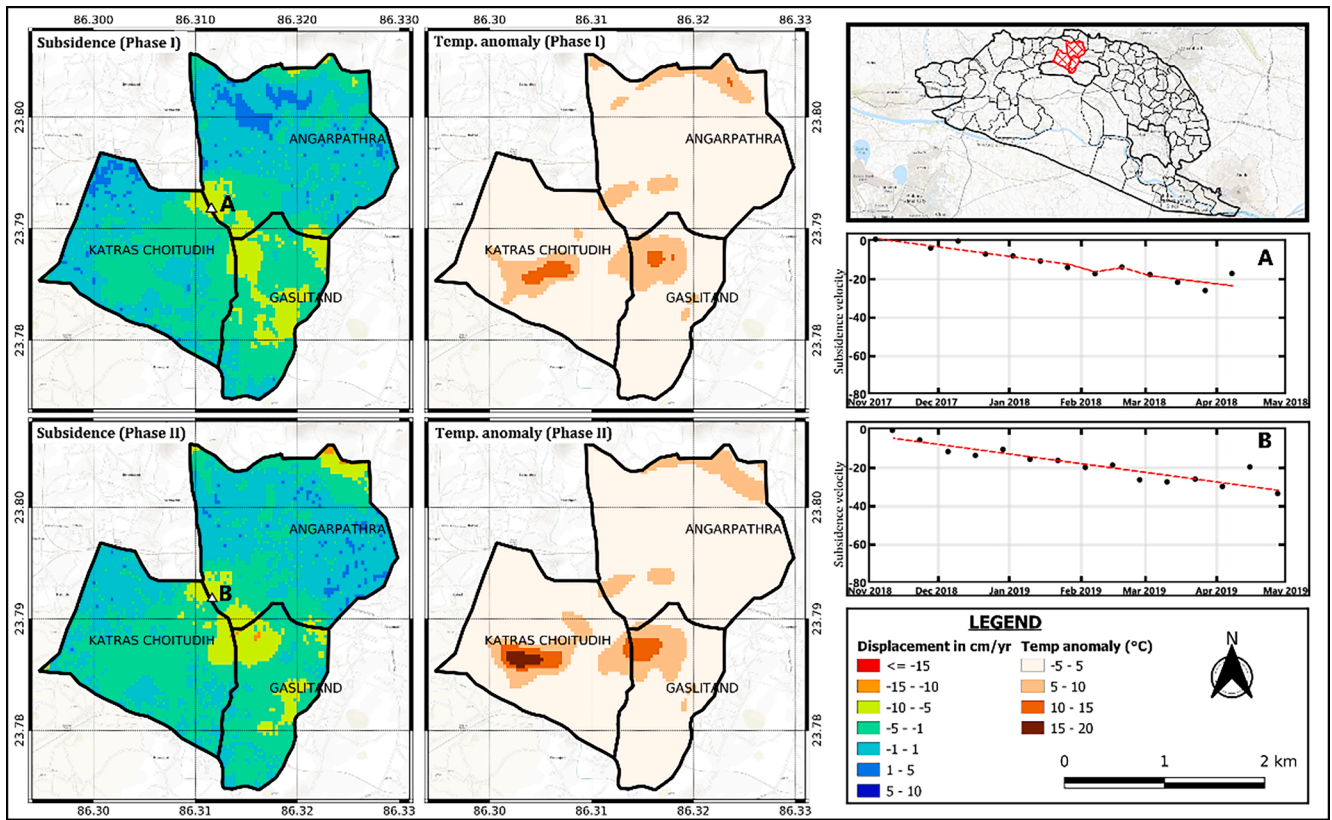


Fig. 9. Spread of coal fire and subsidence hazards in Katras Choituidih, Gaslitand, Angarapatra collieries.

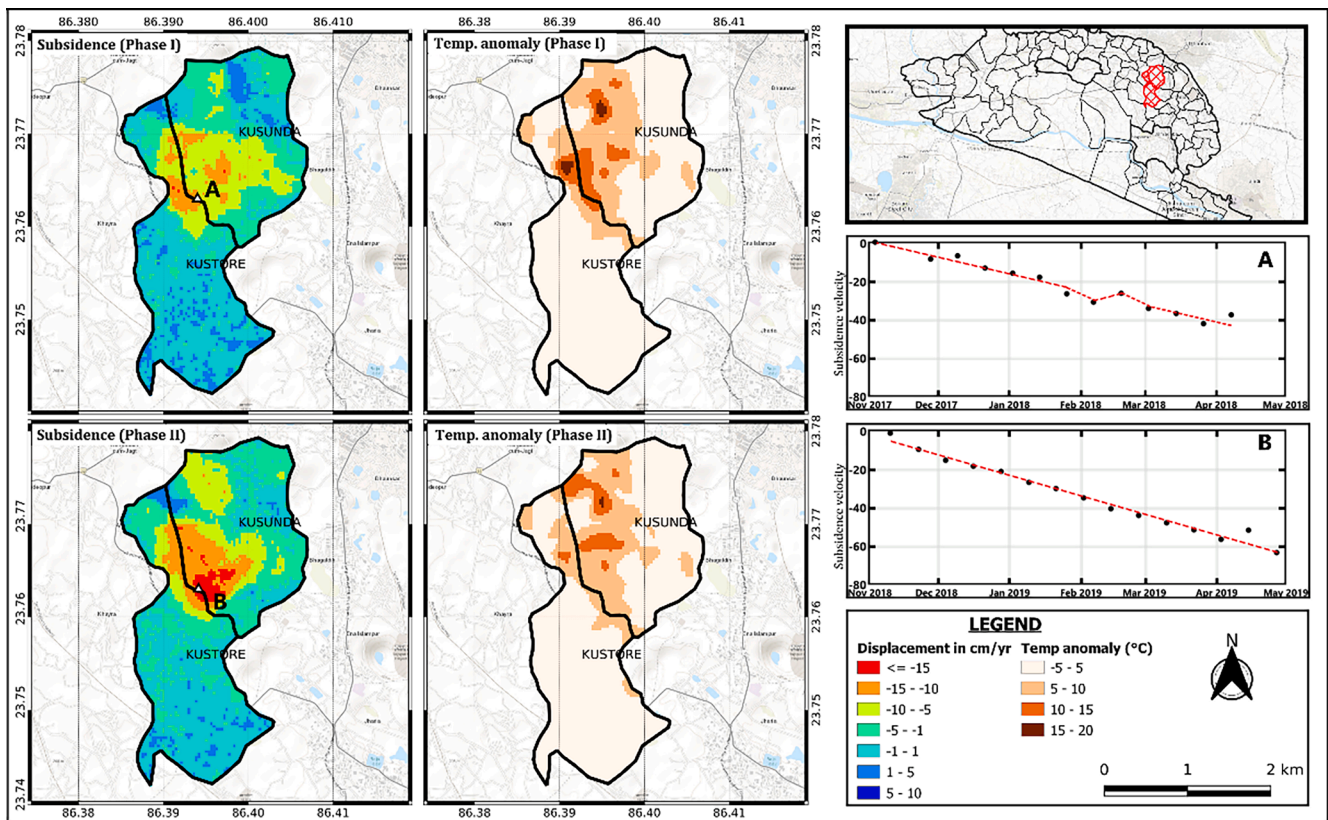


Fig. 10. Spread of coal fire and subsidence hazards in Kusunda and Kustore collieries.

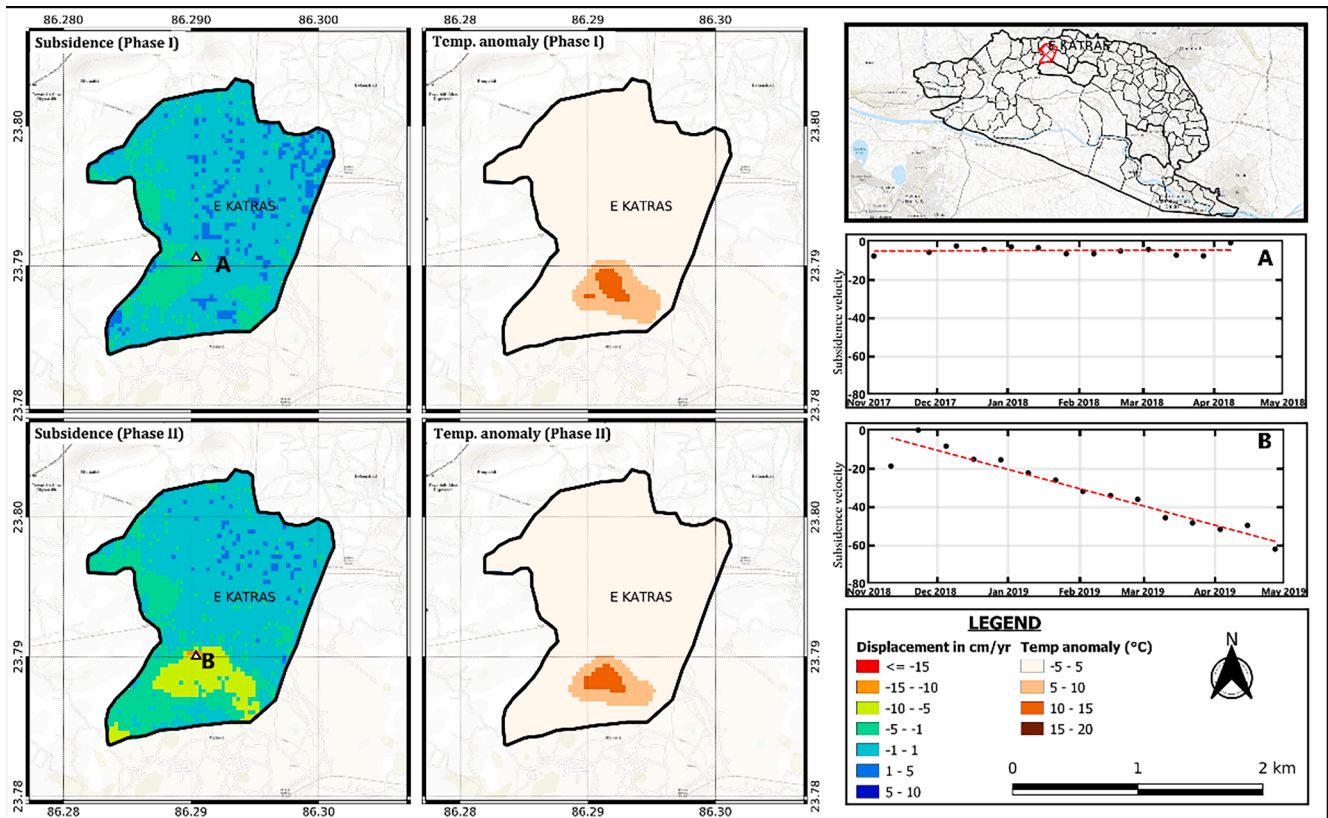


Fig. 11. Spread of coal fire and subsidence hazards in East Katras colliery.

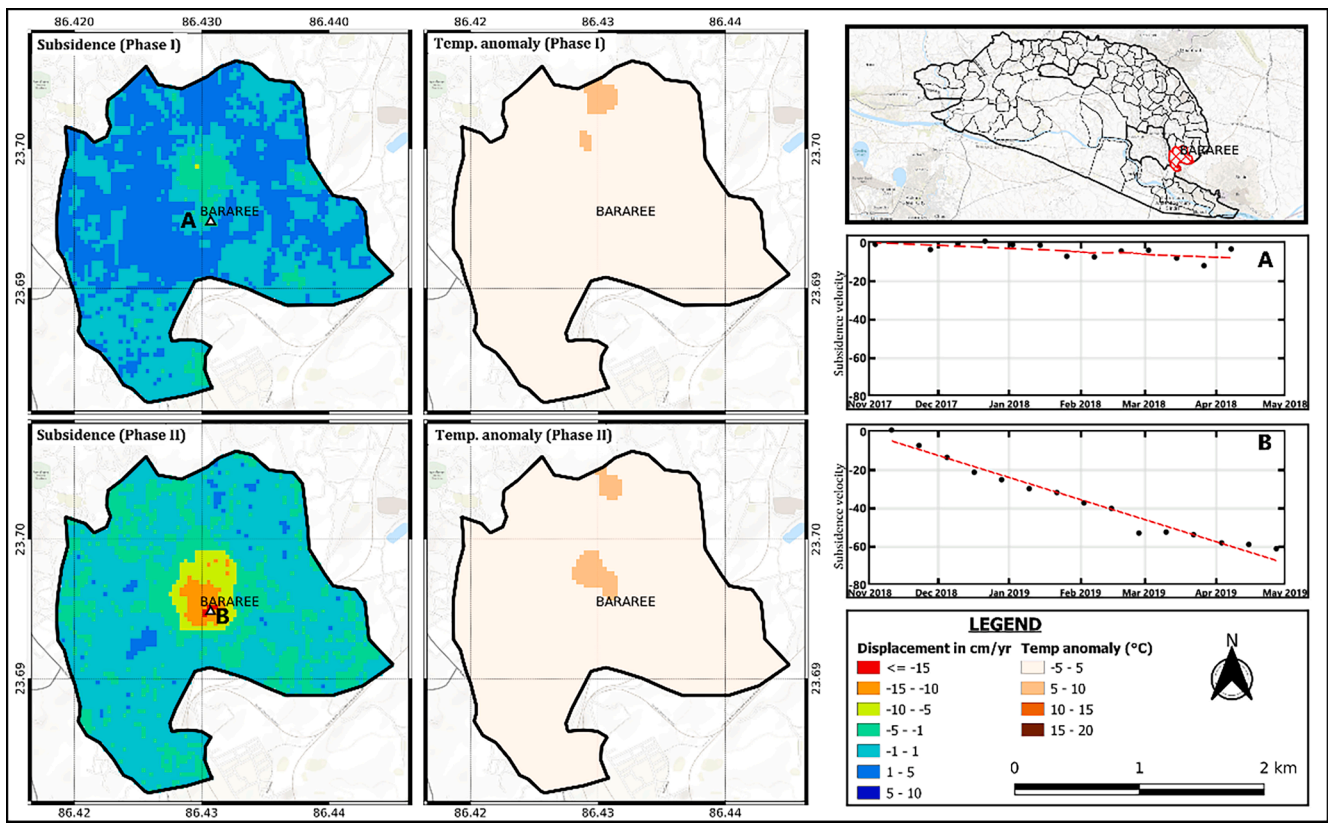


Fig. 12. Spread of coal fire and subsidence hazards in Bararee colliery.

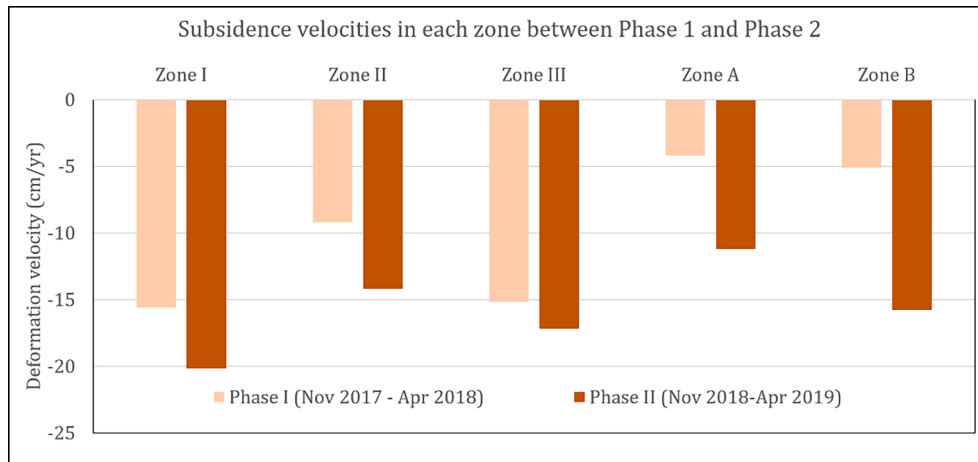


Fig. 13. Subsidence velocities in each zone between Phase 1 and Phase 2.

the coal fires towards Ram Kanali colliery in the second phase. The subsiding area in Ram Kanali is also increased. Another subsiding area with an intensity of more than 10 cm/yr. broke out in West Mudidih in the second phase, partly overlapping with the coal fire area noticeable in both phases.

4.3.2. Zone-II (Katras Choitudih, Gaslitand, Angarapatra)

Katras Choitudih, Gaslitand, and Angarapatra are three collieries that form zone-II (Fig. 9). The major part of the subsidence zone lay in Gaslitand and extended towards the other two collieries. In phase-I, the subsidence is scattered over the Gaslitand colliery. However, in Phase-II, it is more concentrated at the tri-junction of three collieries. Time-series graphs show that subsidence velocity shows a slight increase in the

second phase. Coal fires show an intensified pattern with a significant rise in Katras Choitudih in the second phase of the study. The subsidence phenomenon is expanding outwards, posing a severe threat to the lives of people residing within half a kilometre from the subsidence zone. Also, a new temperature anomaly zone is emerging and intensifying in the Katras Choitudih, which may lead to subsidence soon.

4.3.3. Zone-III (Kusunda and Kustore)

Subsidence zone-III of the study area lies in the Kusunda colliery and is also extended to the Kustore colliery along the border (Fig. 10). Kustore village lies just beside the subsidence zone. Over 1.5 sq. km of area is affected by subsidence and coal fires in this zone. Out of all the subsidence zones analyzed so far, this is the most significant one in the

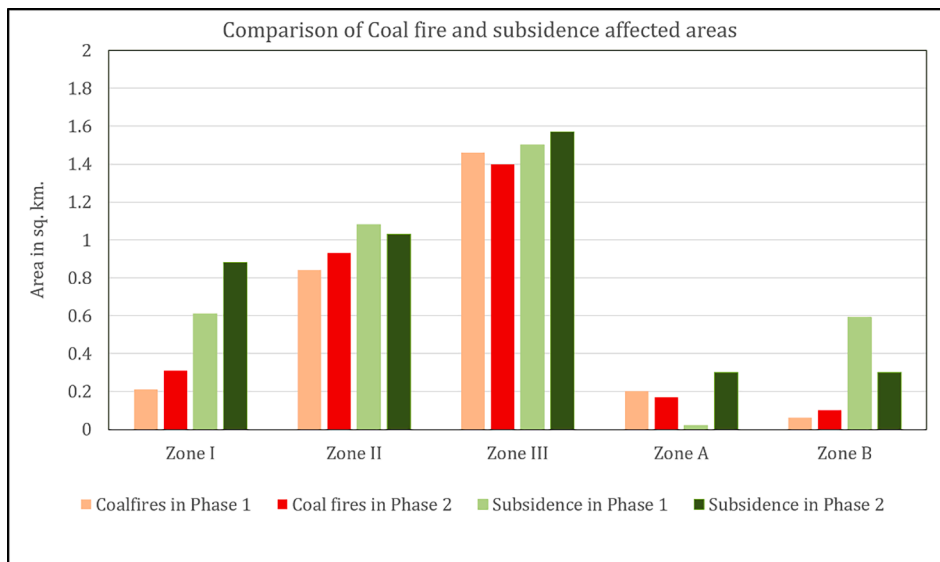


Fig. 14. Comparison of Coal fire and subsidence affected areas between Phase 1 and Phase 2.

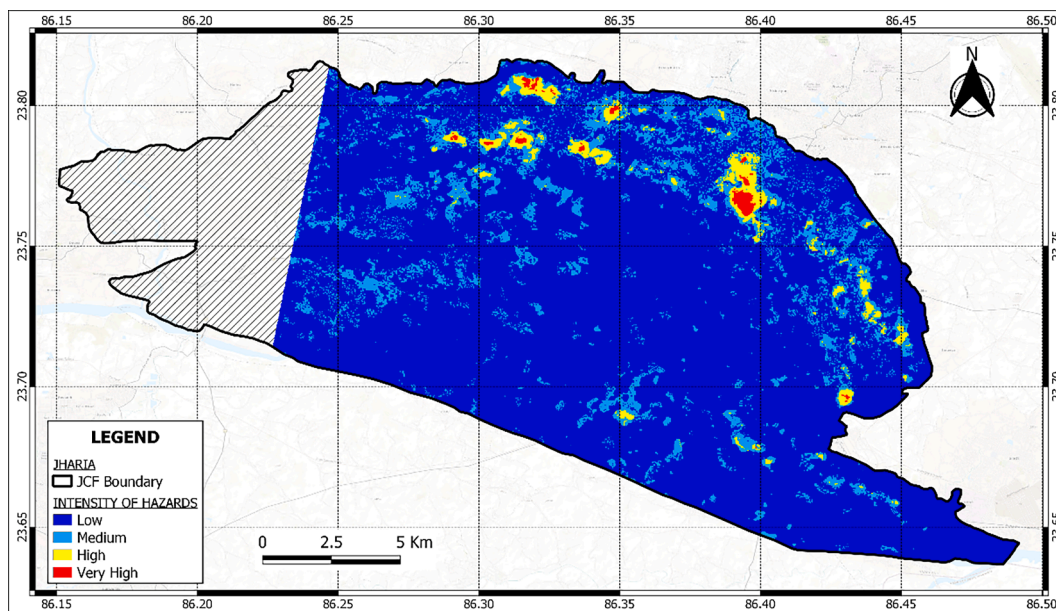


Fig. 15. The extent of subsidence and coal fires in Jharia Coalfields.

Table 3
Spatial coverage of the subsidence and coal fire hazards over different types of land cover.

		mines	settlements	transportation	Others	Total
Hazard intensity	low	93.12	28.60	2.72	144.97	269.42
	medium	17.31	4.15	0.38	18.34	40.18
	high	5.28	0.30	0.04	1.68	7.31
	very high	1.02	0.01	0.00	0.12	1.16

study area, with a subsidence velocity of 15 cm/yr in the first phase and an increased velocity of 17 cm/yr in the second phase. It poses a significant threat to the villages nearby, less than 200 m away from the subsiding area. The northern part of the Kusunda colliery, where subsidence was minimal, but coal fires were prominent in Phase-I manifests subsidence in Phase-II. The subsidence phenomenon is also extending towards the south. The subsidence velocity increased in the second phase while the coal fires continue to burn the coal.

4.3.4. Zone-A (East Katras)

This is an emerging subsidence zone in an area with a history of active coal fires (Fig. 11). This zone is spread over an area of 0.3 sq. km in East Katras colliery in the central part of the Jharia coalfields. The affected zone is less than half a kilometre far from the settlements in Malkera village. However, there seems to be a minimal immediate threat to the settlements. Negligible subsidence is seen in the first phase of the study, while there was a notable presence of coal fires. In the second

Table A1
Minimum, maximum and reference mean temperature over the study area.

S No	Date (Phase-I)	Temperature (°C)			Date (Phase-II)	Temperature (°C)		
		Min	Max	Reference		Min	Max	Reference
1	06-Nov-2017	23.9	48.9	29.3	09-Nov-2018	21.5	48.0	25.3
2	22-Nov-2017	20.6	48.8	25.0	25-Nov-2018	20.1	47.0	24.2
3	24-Dec-2017	18.2	40	21.1	11-Dec-2018	0.6	41.0	20.0
4	09-Jan-2018	15.6	42.2	19.2	27-Dec-2018	2.2	43.2	18.6
5	25-Jan-2018	18.0	45.8	23.2	12-Jan-2019	16.3	45.1	19.9
6	26-Feb-2018	22.8	48.8	30.3	13-Feb-2019	19.9	46.0	24.4
7	14-Mar-2018	25.5	55.4	36.5	01-Mar-2019	18.7	48.1	23.1
8	30-Mar-2018	28.3	59	38.8	17-Mar-2019	22.7	47.3	28.5
9	15-Apr-2018	27.4	55.6	36.9	02-Apr-2019	27.8	54.7	35.6

Table A2
SAR data from Sentinel-1 imagery obtained for phase-I PS analysis.

Descending Data				Ascending Data			
S No	Date	Baseline (m)	Inc. Angle	S No	Date	Baseline (m)	Inc. Angle
1	03-Nov-2017	37	55.740	1	12-Nov-2017	41	59.110
2	15-Nov-2017	-17	50.242	2	24-Nov-2017	-28	46.450
3	27-Nov-2017	-12	45.560	3	06-Dec-2017	126	42.934
4	09-Dec-2017	-69	36.670	4	18-Dec-2017	100	39.063
5	21-Dec-2017	18	36.305	5	30-Dec-2017	149	34.962
6	02-Jan-2018	-19	32.210	6	11-Jan-2018	50	37.326
7	14-Jan-2018	11	30.759	7	23-Jan-2018*	0	45.315
8	26-Jan-2018	-58	32.696	8	04-Feb-2018	9	32.625
9	07-Feb-2018*	0	39.485	9	16-Feb-2018	26	31.727
10	19-Feb-2018	41	30.423	10	28-Feb-2018	29	32.756
11	03-Mar-2018	64	30.169	11	12-Mar-2018	59	35.953
12	15-Mar-2018	21	33.939	12	24-Mar-2018	70	38.231
13	27-Mar-2018	-36	37.860	13	05-Apr-2018	87	44.478
14	08-Apr-2018	-49	50.949	14	17-Apr-2018	95	47.636
15	20-Apr-2018	-90	37.420	15	29-Apr-2018	93	61.652

*master image.

phase, time-series graphs highlight that the subsidence was accelerated to nearly 11 cm/yr in East Katras. Coal fires have been consistent in both phases.

4.3.5. Zone-B (Bararee)

Coal fires and subsidence were minimal in the first phase in the Bararee colliery, which forms Zone-B (Fig. 12). However, in the next phase, both the coal fires and the subsidence are noticeable. Subsidence is accelerated from less than 5 cm/yr to 15 cm/yr within a year. The subsidence zone is towards the southwest of the coalfields, considerably away from the settlements. There is a good correlation between the area occupied by coal fires and the subsidence area in the region. Subsidence is far more intense than the coal fire phenomenon probably due to

Table A3
SAR data from Sentinel 1 imagery obtained for phase-II PS analysis.

Descending Data				Ascending Data			
S No	Date	Baseline (m)	Inc. Angle	S No	Date	Baseline (m)	Inc. Angle
1	10-Nov-2018	-22	52.125	1	07-Nov-2018	71	42.437
2	22-Nov-2018	-57	41.666	2	19-Nov-2018	-2	45.038
3	04-Dec-2018	-35	38.325	3	01-Dec-2018	-13	40.114
4	16-Dec-2018	-159	27.667	4	13-Dec-2018	33	34.946
5	28-Dec-2018	-28	37.165	5	25-Dec-2018	-55	42.147
6	09-Jan-2019	-57	32.953	6	06-Jan-2019	50	35.326
7	21-Jan-2019	11	34.407	7	18-Jan-2019*	0	42.098
8	02-Feb-2019*	0	42.229	8	30-Jan-2019	-31	34.583
9	14-Feb-2019	-113	34.192	9	11-Feb-2019	-19	36.667
10	26-Feb-2019	-35	49.698	10	23-Feb-2019	-66	34.733
11	10-Mar-2019	37	33.206	11	07-Mar-2019	-87	35.491
12	22-Mar-2019	54	31.019	12	19-Mar-2019	-16	40.843
13	03-Apr-2019	67	31.476	13	31-Mar-2019	-85	40.952
14	15-Apr-2019	-33	45.495	14	12-Apr-2019	7	50.882
15	27-Apr-2019	9	46.731	15	24-Apr-2019	-113	41.296

*master image

Table A4
Area covered by Coal fires and subsidence in various intensities in JCF.

	Coal fires (sq. km.)				Total	
	low	medium	high	very high		
Subsidence(sq. km.)	low	126.00	49.40	1.15	0.10	176.65
	medium	93.99	37.56	3.12	0.55	135.22
	high	1.31	2.21	1.15	0.33	4.99
	very high	0.10	0.48	0.53	0.09	1.19
	Total	221.40	89.64	5.95	1.07	318.06

combination of different causes. A coal fire zone in the northern part of the colliery is consistent throughout the study period. However, the site has not subsided. Though this needs further investigation, the possibility of subsidence in the future also needs to be considered.

4.3.6. Subsidence intensity

In Fig. 13, the graph presents the acceleration patterns for all the zones between the phases. All the subsidence zones show considerable acceleration. Zone-A and Zone-B have a very high acceleration rate, and the subsidence velocity more than doubled in just one year. Zone-I and Zone-III show an intense subsidence phenomenon with velocities of nearly 20 cm/yr.

4.3.7. The area occupied by coal fires and subsidence hazards

A graph comparing the area affected by subsidence and coal fires for both phases is shown in Fig. 14. The graph shows a clear association of the area affected by coal fires with that of subsidence. In Zone-I, the area occupied by coal fires is considerably less than that of land subsidence. This can be due to other factors such as undocumented mining, wearing out of pillars and weak soils underneath, or the history of coal fires in the region. Subsidence and coal fires are spread over a vast area in Zone-II and Zone-III and highlight the need for immediate management of the collieries. The subsidence in Zone-A, which was almost non-existent in phase-I, occupied nearly 0.3 sq. km in the second phase.

Apart from these five zones, Tetulmari, Mudidih and Kankanee collieries are also affected by the subsidence and coal fires. In the Tetulmari, a small subsidence zone subsiding at 10 cm/yr occupied an area of 0.4 sq. km. Coal fires are spreading towards the adjacent colliery, Sendra Bansjora. Though the subsidence was not visible in Sendra Bansjora, the spread of coal fires in itself is a considerable threat. Similarly, Kankanee and Mudidih are affected by the coal fires. While the subsidence was noticeable in Kankanee, a new subsidence zone emerged in the neighbouring colliery, Mudidih, extending the subsidence towards the northwest.

4.4. Hazard zonation and vulnerability analysis

Fig. 15 provides a visual representation of the areas affected by the varying intensities of coal fires and land subsidence in the JCF. Almost all major hazard-prone zones are in the northern and north-eastern parts of the coalfields. Several residential areas in the immediate vicinity are vulnerable to the coal-fire induced subsidence. Out of 318 sq. km. the area analyzed in total; areas classified as under high-hazard occupy 7.3 sq. km. while the 40.2 sq. km. are under medium hazard areas. The rest of the 269.4 sq. km. is classified as areas with minimal hazards. The area classified as a very high hazard where both the coal fires and land subsidence hazards are prominent is 1.2 sq km. Detailed calculation of affected areas is given in Table A4. A majority of the hazard-prone areas are in and around the five zones discussed above. A significant part of medium-hazard zones belongs to residential areas around the severely affected coal mine areas. The residential areas, transportation networks, and the coal mines belonging to these high and medium hazard-prone zones require considerable scrutiny to manage the hazards efficiently and provide a safer environment for uninterrupted economic activities and livelihoods.

Later, different type of land cover areas under the influence of these hazards is calculated and presented in Table 3. The results put forth some critical points of concern. First, most of the very high hazard area is over the coal mines and slowly expanding towards the neighbouring settlements. More than 5% of coal mines are classified as high or very high hazard areas. Considering the size of the JCF, 5% is very significant in terms of the number of workers, quantity of affected coal reserves, and other resources. Transportation lines are not severely affected by the hazards. But, transportation lines under medium hazard zones require scrutiny as they are crucial for transporting the coal. The other regions include water sources, vegetation and forests where the human presence

is minimal. The majority of these areas are far away from the coal mines.

The results obtained are in good agreement with the previous studies and newspaper reports. In 2014, several houses in the Katras block, which covers collieries from Zone-I and Zone-II, subsided after developing cracks over several days (Gupta, 2014). In Dec 2020, a woman was sucked into subsiding land in Kusunda Colliery (Network, 2020). Riyas et al., 2021 has observed subsidence in several collieries in JCF with maximum subsidence of more than 22 cm/yr between 2017 and 2020, with a high intense subsidence phenomenon in Kusunda colliery showing a good correlation with the observations presented in the current study. Recent incidents of damages to houses are reported in the Lodna colliery, where subsidence and coal fires are observed in small pockets (TelegraphIndia, 2020).

Roy et al., 2015 has identified Kusunda, Katras-Mudidih, Shatabdi, Kujama and Nadkurkhee-Jayramdih as major coal fire areas. Coal fire in the Shatabdi mine is confined to small pockets. Das, 2016 has observed that Kusunda, Kujama, Bararee and Ena are the major collieries affected by coal fires. They noted that the Nadkurkhee fire is controlled by dumping fine-grained fly ash to stop the oxygen supply. Bharat Coking Coal Limited, which manages the mining operations at JCF, reported in 2018 that Kusunda, Tisra, Lodna, Katras, Gaslitand and Mudidih were most affected by coal fires, as observed from field surveys (Kumar et al., 2018). The other fire areas, including Block II OCP, Shatabdi OCP, have diminished between 2012 and 2017, as reported by them. During the same period, the total extent of coal fires is increased by 50% to 3.28 sq km. In our study, we have identified the presence of coal fires in almost all the locations mentioned above. In addition, we have also observed the significant presence of coal fires in Bararee, Angarapatra, Keshalpur, Ramkanali and West Mudidih.

Considering the locations of the new zones, we can infer that the hazards are extending beyond the North and north-eastern sections of the coalfields towards the southern region. In total, a significant spatial correlation between the subsidence and coal fires is observed, with nearly 80% of the subsiding area in the coalmines also affected by coal fires, pushing the hypothesis of coal fires to be the driving force for the subsidence phenomenon in the mining region. Some subsidence zones extending towards the settlements, transportation networks, and other infrastructure are a matter of concern. Even though most of the areas affected by coal fires and subsidence are inside the coal mines, the adverse effects of these hazards at such a massive scale can be far-reaching. Loss of coal reserves, environmental degradation, dilapidated working conditions, and ill effects on the health of the nearby population, to mention a few. Our study can form a basis to focus on the critical collieries for further studies and in implementing disaster management measures.

Faster decorrelation and atmospheric interactions in the study area restrict the continuous analysis for a more extended period. Hence, the dry season is considered the most suitable for the study. There are some limitations in the current study. The 100 m spatial resolution of TIR data may hide fires in smaller regions and hinder their monitoring leading to the densification of new fire zones even before they are noticed. The maximum detectable deformation in InSAR is limited to half the wavelength of the sensor. For sentinel 1, this is 2.7 cm between successive acquisitions or 42.6 cm per year (Crosetto et al., 2016). Further, any unwrapping error would lead to the underestimation of deformation in the data. While we do not exclude the presence of unwrapping errors at some pixels, we did our best to check the results carefully and removed those interferograms exhibiting phase unwrapping errors during PS analysis. Besides, the PS technique assumes that displacement is linear between the successive image acquisitions, which is 12 days for Sentinel-1. Any non-linearity within 12 days could be masked out by InSAR analysis due to limited temporal sampling. Future SAR satellite missions with shorter revisit time may overcome this and help capture the possible highly non-linear deformation in mining areas. Though Sentinel-1 A started its operation in 2014, the datasets for the current study area are available only from 2017. However, this can be overcome

in the coming years as the data keeps growing.

5. Conclusions

In conclusion, we have demonstrated the efficiency of multi-sensor remote sensing data to estimate and monitor coal fire-induced land subsidence in Jharia coalfields. With thermal anomaly mapping using Landsat 8 TIR imagery and Persistent scatterer analysis of Sentinel imagery using the StaMPS method, we have estimated the intensity, spatial coverage and temporal evolution of the coal fires and land subsidence in Jharia Coalfields and evaluated the correlation between the two. The study is conducted in two phases, each covering a different period, and the change in hazard pattern between the phases was analyzed. The findings exhibit a positive correlation between the subsidence velocity and temperature anomaly in the study area. The coal fires and subsidence are spread across northern and eastern parts of the coalfields and extend towards the south. The results show several localized subsidence zones subsiding at a rate of 10 cm/yr to 20 cm/yr. A significant spatial correlation between the subsidence and coal fires is observed, with nearly 80% of the subsiding area in the coal mines also affected by coal fires. The results show that more than 5% of coal mines are severely affected by the hazards, with Kusunda, Keshalpur and Bararee collieries being the most critically affected zones in the Coal mines. Several subsidence zones close to the residential zones is a matter of concern. Our study can form a basis to focus on the critical collieries for further studies and in implementing disaster management measures. Further, to understand a complete picture of factors leading to subsidence in Jharia, the effect of other causes such as illegal mining, abandoned and aged mines, inundation, and geological parameters can be studied. In closing, the potential of multi-sensor data in building a safer and sustainable ecosystem around the coal mines has been established.

CRedit authorship contribution statement

Vamshi Karanam: Conceptualization, Methodology, Software, Formal analysis, Investigation, Writing - original draft, Visualization, Funding acquisition. **Mahdi Motagh:** Conceptualization, Methodology, Validation, Writing - review & editing, Resources, Supervision, Project administration. **Shagun Garg:** Conceptualization, Visualization, Writing - review & editing. **Kamal Jain:** Conceptualization, Resources, Writing - review & editing, Supervision, Project administration.

Declaration of Competing Interest

The authors declare that they have no known competing financial interests or personal relationships that could have appeared to influence the work reported in this paper.

Acknowledgements

This work was supported in part by the German Academic Exchange Service (DAAD) under Grant reference number 91755744. The authors acknowledge the European Space Agency (ESA) for providing Sentinel-1 datasets and the National Aeronautics and Space Administration (NASA) for providing Landsat-8 datasets. We thank the two anonymous reviewers for their helpful suggestions and comments.

Appendix A

See Table A1–A4.

Appendix B. Supplementary data

Supplementary data to this article can be found online at <https://doi.org/10.1016/j.jag.2021.102439>.

References

- Agarwal, V., Kumar, A., Gomes, L.R., Marsh, S., 2020. Monitoring of Ground Movement and Groundwater Changes in London Using InSAR and GRACE. *Appl. Sci.* 10, 8599. <https://doi.org/10.3390/app10238599>.
- Awasthi, S., Jain, K., Mishra, V., Kumar, A., 2020. An approach for multi-dimensional land subsidence velocity estimation using time-series Sentinel-1 SAR datasets by applying persistent scatterer interferometry technique. *Geocarto Int.* 1–32. <https://doi.org/10.1080/10106049.2020.1831624>.
- Bekaert, D.P.S., Walters, R.J., Wright, T.J., Hooper, A.J., Parker, D.J., 2015. Statistical comparison of InSAR tropospheric correction techniques. *Remote Sens. Environ.* 170, 40–47. <https://doi.org/10.1016/j.rse.2015.08.035>.
- Berardino, P., Fornaro, G., Lanari, R., Sansosti, E., 2002. A new algorithm for surface deformation monitoring based on small baseline differential SAR interferograms. *IEEE Trans. Geosci. Remote Sens.* 40, 2375–2383. <https://doi.org/10.1109/TGRS.2002.803792>.
- Blasco, J.M.D., Fomelis, M., Stewart, C., Hooper, A., 2019. Measuring urban subsidence in the Rome Metropolitan Area (Italy) with Sentinel-1 SNAP-StaMPS Persistent Scatterer Interferometry. *Remote Sens.* 11, 1–17. <https://doi.org/10.3390/rs11020129>.
- Bódis, K., Kougiás, I., Taylor, N., Jäger-Waldau, A., 2019. Solar Photovoltaic Electricity Generation: A Lifeline for the European Coal Regions in Transition. *Sustainability* 11, 3703. <https://doi.org/10.3390/su11133703>.
- Borah, S.B., Chatterjee, R.S., Thapa, S., 2017. Detection of underground mining induced land subsidence using Differential Interferometric SAR (D-InSAR) in Jharia coalfields 00602621, 1–6.
- Bringemeier, D., 2012. Inrush and mine inundation—A real threat to Australian coal mines. In: *Proceedings of the International Mine Water Association Annual Conference*, Bunbury, Australia.
- Cell, R.S., 2017. *Vegetation Cover Mapping of Jharia Coalfield based on Satellite Data of the Year- 2016*. DHANBAD.
- Chatterjee, R.S., 2006. Coal fire mapping from satellite thermal IR data – A case example in Jharia Coalfield, Jharkhand, India. *ISPRS J. Photogramm. Remote Sens.* 60, 113–128. <https://doi.org/10.1016/j.isprsjprs.2005.12.002>.
- Chatterjee, R.S., Wahiduzzaman, M., Shah, A., Raju, E.V.R., Lakhera, R.C., Dadhwal, V. K., 2007. Dynamics of coal fire in Jharia Coalfield, Jharkhand, India during the 1990s as observed from space. *Curr. Sci.* 92, 61–68.
- Chatterjee, R.S., Lakhera, R.C., Dadhwal, V.K., 2010. InSAR coherence and phase information for mapping environmental indicators of opencast coal mining: A case study in Jharia Coalfield, Jharkhand, India. *Can. J. Remote Sens.* 36, 361–373. <https://doi.org/10.5589/m10-047>.
- Chatterjee, R.S., Thapa, S., Singh, K.B., Varunakumar, G., Raju, E.V.R.R., 2015. Detecting, mapping and monitoring of land subsidence in Jharia Coalfield, Jharkhand, India by spaceborne differential interferometric SAR, GPS and precision levelling techniques. *J. Earth Syst. Sci.* 124, 1359–1376. <https://doi.org/10.1007/s12040-015-0606-5>.
- Chatterjee, R.S., Singh, K.B., Thapa, S., Kumar, D., 2016. The present status of subsiding land vulnerable to roof collapse in the Jharia Coalfield, India, as obtained from shorter temporal baseline C-band DInSAR by smaller spatial subset unwrapped phase profiling. *Int. J. Remote Sens.* 37, 176–190. <https://doi.org/10.1080/2150704X.2015.1126376>.
- Crosetto, M., Monserrat, O., Cuevas-González, M., Devanthery, N., Crippa, B., 2016. Persistent Scatterer Interferometry: A review. *ISPRS J. Photogramm. Remote Sens.* 115, 78–89. <https://doi.org/10.1016/j.isprsjprs.2015.10.011>.
- Das, G.D.R., 2016. *Land Use/Land Cover Status relating the Coal fire of Jharia Coal Field - An Analytical Case Study by RS-GIS Techniques*. *Int. J. Sci. Res.* 5, 1–11.
- Deng, Y., Song, L., Zhou, Z., Liu, P., 2017. An Approach for Understanding and Promoting Coal Mine Safety by Exploring Coal Mine Risk Network. *Complexity* 2017, 1–17. <https://doi.org/10.1155/2017/7628569>.
- Gangopadhyay, P.K., Van der Meer, F., Van Dijk, P.M., Saha, K., 2012. Use of satellite-derived emissivity to detect coalfire-related surface temperature anomalies in Jharia coalfield, India. *Int. J. Remote Sens.* 33, 6942–6955. <https://doi.org/10.1080/01431161.2012.695093>.
- Gupta, A., 2014. *About 50 houses subside in underground coal fire in Jharkhand's Jharia*. *Down To Earth*.
- Gupta, N., Syed, T.H., Athipho, A., 2013. Monitoring subsurface coal fires in Jharia coalfield using observations of land subsidence from differential interferometric synthetic aperture radar (DInSAR). *J. Earth Syst. Sci.* 122, 1249–1258. <https://doi.org/10.1007/s12040-013-0355-2>.
- Haghighi, M.H., Motagh, M., 2017. Sentinel-1 InSAR over Germany: Large-scale interferometry, atmospheric effects, and ground deformation mapping. *ZfV - Zeitschrift für Geodäsie. Geoinf. und Landmanagement* 142, 245–256. <https://doi.org/10.12902/zfv-0174-2017>.
- Hooper, A., Spaans, K., Bekaert, D., Cuenca, M.C., Arikani, M., Oyen, A., 2010. *StaMPS/MTI manual*. Delft Inst. Earth Obs. Sp. Syst. Delft Univ. Technol. *Kluyverweg 1*, 2629.
- Haghshenas Haghighi, M., Motagh, M., 2019. Ground surface response to continuous compaction of aquifer system in Tehran, Iran: Results from a long-term multi-sensor InSAR analysis. *Remote Sens. Environ.* 221, 534–550. <https://doi.org/10.1016/j.rse.2018.11.003>.
- Hooper, A., Bekaert, D., Spaans, K., Arikani, M., 2012. Recent advances in SAR interferometry time series analysis for measuring crustal deformation. *Tectonophysics* 514–517, 1–13. <https://doi.org/10.1016/j.tecto.2011.10.013>.
- Jiang, L., Lin, H., Ma, J., Kong, B., Wang, Y., 2011. Potential of small-baseline SAR interferometry for monitoring land subsidence related to underground coal fires:

- Wuda (Northern China) case study. *Remote Sens. Environ.* 115, 257–268. <https://doi.org/10.1016/j.rse.2010.08.008>.
- Kuenzer, C., Zhang, J., Hirner, A., Bo, Y., Jia, Y., Sun, Y., 2008. Multitemporal in-situ mapping of the Wuda coal fires from 2000 to 2005 – assessing coal fire dynamics. *ERSEC Ecological Book Series*. 132–148.
- Kumar, S.S.S., Pathak, P., 2001. Disaster Management, a Case of a Coal Mine.
- Kumar, D.K.V., Martha, D.T.R., Roy, P., 2018. Delineation of surface coal fire and land subsidence in the Jharia Coalfield, Dhanbad. *Jharkhand From Remote Sensing Data, Dehradun*.
- Limited, B.C.C., 2020. Annual Report and Accounts 2019-20. Jharia.
- Liu, J., Wang, Y., Li, Y., Dang, L., Liu, X., Zhao, H., Yan, S., 2019. Underground Coal Fires Identification and Monitoring Using Time-Series InSAR with Persistent and Distributed Scatterers: A Case Study of Miqian Coal Fire Zone in Xinjiang, China. *IEEE Access* 7, 164492–164506. <https://doi.org/10.1109/ACCESS.2019.2952363>.
- Massonnet, D., Feigl, K.L., 1998. Radar interferometry and its application to changes in the Earth's surface. *Rev. Geophys.* 36, 441–500. <https://doi.org/10.1029/97rg03139>.
- Mishra, R.K., Pandey, J.K., Pandey, J., Kumar, S., Roy, P.N.S., 2020. Detection and Analysis of Coal Fire in Jharia Coalfield (JCF) Using Landsat Remote Sensing Data. *J. Indian Soc. Remote Sens.* 48, 181–195. <https://doi.org/10.1007/s12524-019-01067-6>.
- Motagh, M., Djamour, Y., Walter, T.R., Wetzel, H.-U., Zschau, J., Arabi, S., 2007. Land subsidence in Mashhad Valley, northeast Iran: results from InSAR, levelling and GPS. *Geophys. J. Int.* 168, 518–526. <https://doi.org/10.1111/j.1365-246X.2006.03246.x>.
- Motagh, M., Shamschiri, R., Haghshenas Haghghi, M., Wetzel, H.-U., Akbari, B., Nahavandchi, H., Roessner, S., Arabi, S., 2017. Quantifying groundwater exploitation induced subsidence in the Rafsanjan plain, southeastern Iran, using InSAR time-series and in situ measurements. *Eng. Geol.* 218, 134–151. <https://doi.org/10.1016/j.enggeo.2017.01.011>.
- Motagh, M., Walter, T.R., Sharifi, M.A., Fielding, E., Schenk, A., Anderssohn, J., Zschau, J., 2008. Land subsidence in Iran caused by widespread water reservoir overexploitation. *Geophys. Res. Lett.* 35, L16403. <https://doi.org/10.1029/2008GL033814>.
- Network, T.N., 2020. Woman dies as land subsides in Jharia. *Times of India*.
- Pandey, J., Kumar, D., Singh, V.K., Mohalik, N.K., 2016. Environmental and Socio-Economic Impacts of Fire in Jharia Coalfield, Jharkhand, India: An Appraisal. *Curr. Sci.* 110, 1639. <https://doi.org/10.18520/cs/v110/i9/1639-1650>.
- Pinto, C. d. A., Paradella, W.R., Mura, J.C., Gama, F.F., dos Santos, A.R., Silva, G.G., 2014. Results of the application of persistent scatterers interferometry for surface displacements monitoring in the Azul open pit manganese mine (Carajás Province, Amazon region) using TerraSAR-X data. *Earth Resour. Environ. Remote Sensing/GIS Appl. V.* <https://doi.org/10.1117/12.2067233>.
- Prakash, A., Lokhande, R.D., Singh, K.B., 2010. Impact of rainfall on residual subsidence in old coal mine workings. *J. Environ. Sci. Eng.* 52, 75–80.
- Riyas, M.J., Syed, T.H., Kumar, H., Kuenzer, C., 2021. Detecting and Analyzing the Evolution of Subsidence Due to Coal Fires in Jharia Coalfield, India Using Sentinel-1 SAR Data. *Remote Sens.* 13, 1521. <https://doi.org/10.3390/rs13081521>.
- Rosema, A., van Genderen, J.L., Schalke, H.J.W.G., 1995. Environmental monitoring of coal fires in North China : project identification mission report October 1993, BCRS Repor. ed. Beleidscommissie Remote Sensing (BCRS).
- Rosen, P.A., Hensley, S., Joughin, I.R., Li, F.K., Madsen, S.N., Rodriguez, E., Goldstein, R. M., 2000. Synthetic aperture radar interferometry. *Proc. IEEE* 88, 333–382. <https://doi.org/10.1109/5.838084>.
- Roy, P., Guha, A., Kumar, K.V., 2015. An approach of surface coal fire detection from ASTER and Landsat-8 thermal data: Jharia coal field, India. *Int. J. Appl. Earth Obs. Geoinf.* 39, 120–127. <https://doi.org/10.1016/j.jag.2015.03.009>.
- Saraf, A.K., Prakash, A., Sengupta, S., Gupta, R.P., 1995. Landsat-tm data for estimating ground temperature and depth of subsurface coal fire in the jharia coalfield, india. *Int. J. Remote Sens.* 16, 2111–2124. <https://doi.org/10.1080/01431169508954545>.
- Saxena, N.C., 1991. Subsidence management in Jharia coalfield, India. A concept. *IAHS Publ (International Assoc. Hydrol. Sci.)* 181–193. [https://doi.org/10.1016/0148-9062\(92\)94161-j](https://doi.org/10.1016/0148-9062(92)94161-j).
- Singh, K.B., Dhar, B.B., 1997. Sinkhole subsidence due to mining. *Geotech. Geol. Eng.* 15, 327–341. <https://doi.org/10.1007/bf00880712>.
- Singh, A., Raju, A., Pati, P., Kumar, N., 2017. Mapping of Coal Fire in Jharia Coalfield, India: a Remote Sensing Based Approach. *J. Indian Soc. Remote Sens.* 45, 369–376. <https://doi.org/10.1007/s12524-016-0590-5>.
- Stracher, G.B., Taylor, T.P., 2004. Coal fires burning out of control around the world: thermodynamic recipe for environmental catastrophe. *Int. J. Coal Geol.* 59, 7–17. <https://doi.org/10.1016/j.coal.2003.03.002>.
- TelegraphIndia, 2020. Cattle shed, portion of a home cave in at Lodna Colliery area. *Telegr. India*.
- Verma, R.K., Bhui, N.C., Mukhopadhyay, M., 1979. Geology, structure and tectonics of the Jharia Field, India - a three-dimensional coal. *Geoexploration* 17, 305–324. [https://doi.org/10.1016/0016-7142\(79\)90025-5](https://doi.org/10.1016/0016-7142(79)90025-5).
- World Energy Outlook 2018, 2018. World Energy Outlook. OECD. <https://doi.org/10.1787/weo-2018-en>.
- Yu, C., Li, Z., Penna, N.T., 2018. Interferometric synthetic aperture radar atmospheric correction using a GPS-based iterative tropospheric decomposition model. *Remote Sens. Environ.* 204, 109–121. <https://doi.org/10.1016/j.rse.2017.10.038>.
- Zhang, J., Wagner, W., Prakash, A., Mehl, H., Voigt, S., 2004. Detecting coal fires using remote sensing techniques. *Int. J. Remote Sens.* 25, 3193–3220. <https://doi.org/10.1080/01431160310001620812>.
- Zhou, L., Zhang, D., Wang, J., Huang, Z., Pan, D., 2013. Mapping land subsidence related to underground coal fires in the wuda coalfield (Northern China) using a small stack of ALOS PALSAR differential interferograms. *Remote Sens.* 5, 1152–1176. <https://doi.org/10.3390/rs5031152>.